International Journal of Pharmacy and Pharmaceutical Sciences

ISSN- 0975-1491 Vol 8, Issue 3, 2016

Original Article

PREPARATION, CHARACTERISATION AND COLLOIDAL STABILITY OF CHITOSAN-TRIPOLYPHOSPHATE NANOPARTICLES: OPTIMISATION OF FORMULATION AND PROCESS PARAMETERS

ZAHID HUSSAIN, SHARIZA SAHUDIN*

Department of Pharmaceutics, Faculty of Pharmacy, Universiti Teknologi Mara, Puncak Alam Campus, Bandar Puncak Alam, 42300, Selangor, Malaysia
Email: sharizasahudin@gmail.com

Received: 09 Oct 2015 Revised and Accepted: 03 Feb 2016

ABSTRACT

Objective: Chitosan (CS)–tri polyphosphate (TPP)–nano particles (NPs) have been extensively studied during the past few decades due to their well-recognized applicability in various fields. Thus, the present study was aimed to optimise the fabrication conditions for the preparation of CS-TPP-NPs aiming towards smallest possible size, optimal zeta potential and narrow poly dispersity index (PDI), simultaneously.

Methods: CS-TPP-NPs were prepared *via* ionic cross-linking of CS and TPP and were characterized physico-chemically (particle size, zeta potential and PDI) and morphologically. The influence of several formulation conditions (CS concentrations, CS: TPP mass ratio and initial pH of CS solutions) and process parameters (stirring speed, stirring time, ultra-sonication and ultra-centrifugation) on the colloidal characteristics of CS-TPP-NPs were investigated. In addition, the colloidal stability of the prepared NPs was also assessed on storage.

Results: Results clearly identified that the formulation and process parameters showed significant impact on the physico-chemical and morphological characteristics of the CS-TPP-NPs. The CS-TPP-NPs prepared under optimum conditions (CS concentration of 0.2 mg/ml, CS: TPP mass ratio of 7:1, initial pH of CS solution of 4.0, stirred at 700 rpm for 10 min and ultra-centrifuged at 25 000 rpm for 30 min) had shown a mean particle size of ~187±21 nm, zeta potential of+37±3.5 mV, PDI of ~0.28±0.0390 as well as the smooth and round shaped morphology.

Conclusion: The present study describes the optimal circumstances to fabricate the CS-TPP-NPs with finest physico-chemical characteristics and also explore the prospects of manipulation and optimisation of the NPs for intended applications.

Keywords: Chitosan nanoparticles, Ionic cross-linking, Morphology, Ultra-sonication, Ultra-centrifugation, Colloidal stability

INTRODUCTION

Numerous drug delivery systems have been developed from 1980s to date in order to improve drug efficacy, optimize target-specific delivery and to minimize non-target toxic effects. In recent decades, the researcher's orientation is being driven by the polymer-based nanotechnology. The reason for the successfulness of the polymer-based drug delivery is biodegradability and biocompatibility of the synthetic, semi-synthetic and/or natural polymers, which include poly (lactide-co-glycolide) (PLGA) [1], poly(ε-caprolactone) [2], chitosan (CS) [3] and a combination of CS and poly(gamma-glutamic acid) [4]. These types of nano-carriers can potentially: (1) protect the labile compounds from premature degradation, (2) provide controlled and sustained release profile *via* modification of the polymeric matrix [5-7] and (3) increase targeted delivery and thus, reduce non-target toxicities [8,9]. Nano carrier-based delivery had also gained remarkable attention in various fields because of their ability to deliver wide range of active molecules in different body organs and retained for prolonged time periods.

Among several polymers constituting NPs; the natural polymer chitosan (CS), has been well-established in the preparation of NPs because of many advantages such as biodegradability by human enzymes, biocompatibility with wide range of cellular lines and safety profile [10-12]. CS is a natural polysaccharide comprising of co-polymers of glucosamine and N-acetyl glucosamine. It is derived by the partial de acetylation of chitin from crustacean shells. Various techniques have been used to fabricate CS-mediated NPs including, emulsification, ionic cross-linking, and coacervation/precipitation, spray-drying, emulsion droplet coalescence method, reverse micellar method, sieving and ionic gelation methods. However among all, the ionic gelation technique has numerous advantages such as; (1) use of aqueous media; (2) preparation of small size and compact structured particles; (3) control of colloidal characteristics of the NPs by the variation of formulation and process parameters; (4) the possibility of encapsulation of a wide range of molecules for different intended applications.

The mechanism behind the ionic gelation method involves an ionic cross-linking between cations on the backbone of CS and anion such as sodium tri polyphosphate (TPP). In an acidic environment CS becomes positively charged and soluble due to the proton ation of amino groups of glucosamine. Penta sodium tri polyphosphate (TPP) is among the most commonly used poly anion because of its non-toxic and gel forming properties [13, 14]. Positively charged NPs are formed through inter-and intra-cross-linking of the amino groups ($-NH_3^+$) of CS with negatively charged phosphate groups ($-PO_4^-$) of TPP, as reported by Calvo *et al.* [15]. The ionic-gelation method has been extensively studied in various circumstances including, the effect of formulation and process parameters on the colloidal characteristics and stability of NPs [16]. The particle size distribution and zeta potential of NPs greatly depends on the mixing procedure of CS and TPP and their stoichiometry, as well as CS concentration, degree of de acetylation, and molecular weight [16, 17]. The NPs colloidal characteristics are also sensitive to the ionic strength and the initial pH of preparation media [14, 18]. The CS-TPP-NPs because of their biodegradability, low toxicity and bio-compatibility have been frequently studied as a potential delivery system for various compounds such as, drugs [11, 19-22], proteins [23-25], flavonoids [26], essential oils [27, 28] and genes [29].

The current research was executed to investigate the fabrication behaviour of the CS-TPP-NPs at various formulation conditions and process parameters. The colloidal characteristics of the NPs as a function of mean diameter, dispersity index and surface charge were examined by varying key parameters such as CS concentration, CS: TPP mass ratio and initial pH of CS solution. In addition, the effect of stirring rate, ultra-centrifugation and ultra-sonication were also

studied in the preparation, characterization and isolation of the NPs from large particles and agglomerates. Data was further harmonized by using transmission electron microscopy (TEM) to observe morphological changes in the NPs at various preparation conditions. Thus, the aims of the present study were; (a) to evaluate the influence of various formulation and process parameters on the physico-chemical characteristics of prepared NPs, (b) to achieve the optimal conditions for the preparation of CS-TPP-NPs, (c) to fabricate the CS-TPP-NPs of smallest possible mean size, highest possible zeta potential and narrow dispersity index, (d) to determine the swelling behaviour of the prepared NPs, and (d) to assess the colloidal stability of NPs at different storage conditions.

MATERIALS AND METHODS

Materials

CS (MW, 70 kDa; de acetylation degree, 85%) and phosphate buffered saline (PBS) were purchased from Sigma Aldrich Chemicals Co. Ltd. (Kuala Lumpur, Malaysia). TPP was obtained from Merck KGaA Co. Ltd. (Germany). All other chemicals used were of analytical grade and were sourced from laboratories of University Kebangsaan Malaysia (UKM).

Preparation of CS-TPP-NPs

CS-TPP-NPs were prepared *via* ionic cross-linking of CS with TPP in accordance to Calvo *et al.* [15] with slight modifications. CS solution of 2 mg/ml was prepared in acetic acid (1% v/v) at different pH values (3.0, 4.0, 5.0, 6.0, and 7.0). The pH of the mixtures was measured and adjusted with 0.5*M* NaOH or 1 *M* HCl using pH meter (FE20-FiveEasy™, METTLER TOLEDO, USA). CS-TPP-NPs were spontaneously formed by adding 10 ml of TPP solution (0.1% w/v) drop wise into 25 ml of CS solution (2 mg/ml) under vigorous magnetic stirring (700 rpm) for 30 min at room temperature. The effect of magnetic stirring was investigated at various rotations between 200 rpm and 1000 rpm for 30 min. In order to use different CS: TPP mass ratios (1:1 to 10:1), the initial concentration of CS was kept constant while the volume of TPP added was varied. Likewise, CS-TPP-NPs were also prepared at various CS concentrations (0.5, 1.0, 2.0, 3.0, 4.0 and 5.0 mg/ml) using constant TPP concentration (1.0 mg/ml) at room temperature. The resulted CS-TPP-NPs were harvested by ultra-centrifugation using an Optima L-100 XP Ultracentrifuge (Beckman-Coulter, USA) with a NV 70.1 Ti rotor (Beckman-Coulter, USA) for 30 min. After the ultra-centrifugation, sediment and supernatant were separated carefully by removing the supernatant layer for further analysis. The NPs were subsequently lyophilized (Scanvac Cool Safe™, Chemo science, Thailand) at-40 °C for 24 h.

We investigated the effect of several parameters on the CS-TPP-NPs properties. In the first set of experiments, we varied the formulation factors: CS concentrations, CS: TPP mass ratios and the initial pH of CS solutions. In the second set of experiments, we investigated the effect of operating parameters: stirring speed, stirring time, ultra-sonication and ultra-centrifugation on the physico-chemical characteristics of the prepared NPs.

Particle size, zeta potential and PDI

The sediments of the CS-TPP-NPs obtained after ultra-centrifugation were resuspended in distilled water. The average particle size, zeta potential and PDI were then measured using ZS-90 Zetasizer® (Malvern Instruments, UK) on the basis of dynamic light scattering technique. All measurements were performed in triplicates at 25 °C with a detection angle of 90°. Results were reported as mean±standard deviation (SD) (n=3).

Effect of ultra-sonication

Ultra-sonication was performed based on the method reported by Floris *et al.* [30] with slight modification. Ultra-sonic treatments were administered using an ultra-sonic probe with diameter of 20 mm and a 500 W high-intensity ultra-sonic processor (VCX 500, Sonics and Materials Inc., USA) operating at 20 kHz. The CS-TPP-NPs dispersions were placed in 50 ml beakers and ultra-sonicated in ice bath in discontinuous mode in order to avoid temperature fluctuation. The ultra-sonic radiation was interrupted by breaks where the time fraction of both ultrasonic radiation and the break was 0.5 s. The probe was immersed 2 cm deep into the dispersion and ultra-sonicated over a period of 10 min.

Effect of ultra-centrifugation

This experiment was performed to assess the impact of ultra-centrifugation on the physico-chemical and colloidal characteristics of CS-TPP-NPs. For that, the NPs after simultaneous preparation were harvested by a series of ultra-centrifugation speeds (15 000 rpm, 20 000 rpm, 25 000 rpm, 30 000 rpm and 35 000 rpm) using Optima L-100 XP Ultracentrifuge (Beckman-Coulter, USA) with a NV 70.1 Ti rotor (Beckman-Coulter, USA) keeping the ultra-centrifugation time constant at 30 min. The centrifuged/sediment NPs were then re-dispersed in the 2 ml of ultra-pure water and were characterized for mean particle size, zeta potential and size distribution range. The results were reported as mean±SD (n = 3).

Morphological examination

The morphological features of prepared CS-TPP-NPs were examined using high-performance digital imaging transmission electron microscope (TEM) (JEOLH-7650, Hitachi High-Technologies Corp., Tokyo, Japan). For TEM analysis, a drop of CS-TPP-NPs dispersion (in distilled water) was placed onto the copper micro grid which was natively stained by phosphotungstic acid, and was allowed to evaporate and dry at room temperature (25±2 °C). The dried micro grids were then viewed at various resolutions under TEM.

Swelling studies

To assess the swelling behaviour of the prepared CS-TPP-NPs, dry samples (100 mg) of lyophilized NPs were immersed in PBS at different pH values (3.0, 4.0, 5.0, 6.0, 7.0, and 8.0) for 24 h at room temperature, until a swollen equilibrium was achieved. The swollen samples obtained were then collected by filtration, blotted with filter paper for the removal of surface adsorbed water and weighed immediately. The swelling ratios of CS-TPP-NPs were calculated using equation 1 [31]:

$$\text{Swelling ratio } (\%) = \text{Ws} - \frac{\text{Wd}}{\text{Wd}} \times 100 \quad (1)$$

Where, W_s and W_d are the weights of swollen and dry samples, respectively. Results were measured in triplicates (n=3) and were reported as mean±SD.

Colloidal stability

A series of experiments were executed to determine the colloidal stability of CS-TPP-NPs. In this experiment, the NPs were separated from the acidic continuous phase by ultra-centrifugation at 25,000 rpm for 30 min. The separated NPs were then washed with ultra-pure water 2 times by re-suspension and ultra-centrifugation cycles consecutively. The NPs were then stored in borosilicate glass vials at room temperature (25±2°C) for 32 d. The aliquots of NPs were collected at various intervals (0, 2, 4, 8, 11, 18, 22, 24, 25 and 32 d). The collected samples were then characterized for mean particle size, PDI, zeta potential and morphological examination. The results were reported as mean±SD (n=3).

Statistical data analysis

The whole data is presented as mean±SD (n=3). Data were analyzed using either paired t-tests or independent t-test and analysis of variance (ANOVA) followed by Tukey's post-hoc analysis. For particle size, zeta potential, swelling ratios and stability studies, a p value<0.05 was considered to indicate a significant difference between the samples tested.

RESULTS AND DISCUSSION

Optimization of CS concentration

CS concentration is perhaps the most important determinant of the physico-chemical characteristics of the CS-TPP-NPs. Fig. 1 showed the effect of CS concentrations on the particle size, zeta potential and PDI of CS-TPP-NPs at constant CS: TPP mass ratio (5:1). The particle size was linearly increased from 122±9 to 227±16 nm by increasing CS concentration from 0.5 to 2 mg/ml (fig. 1a). The particle size was further increased significantly (p<0.05, paired t-test) from 284±23

to 538±32 nm, when CS concentration was increased from 3 to 5 mg/ml. These results were also in agreement with previously published reports[14, 26, 32, 33]. The increase in particle size was expected to be due to the presence of inter-molecular hydrogen bonding (due to–OH groups) and inter-molecular electrostatic repulsion (due to–NH_3^+groups) which exist along the contour of CS [34]. As the concentration of CS increases, more molecules of CS tend to entangle with each other and crosslink with counter ion (TPP) to form a single larger particle [33].

Fig. 1b showed the effect of CS concentration on the surface charge of CS-TPP-NPs. The zeta potential of the CS-TPP-NPs was found to be significantly ($p<0.05$, paired t-test) increased from+19±3 to+52±3 mV, when the CS concentration was increased from 0.5 to 4 mg/ml. However, the surface charge of NPs was decreased suddenly, when CS concentration was increased from 4 to 5 mg/ml as shown in fig. 1b. The increase in zeta potential from 0.5 to 4 mg/ml could be associated with the fact that the positive surface charge on CS-TPP-NPs was mainly due to the residual amine groups on the contour of CS that have not interacted with the TPP ions. Thus, the zeta potential of NPs was increased linearly with increasing the CS concentration as more unneutralised–NH_3^+groups were present on the surface of NPs. However, a slight decrease in the surface charge when the CS concentration was increased from 4 to 5 mg/ml, was expected to be caused by the less H^+ions liberated from the acetic acid ($CH_3COO^-H^+$) which had been fully used up to protonate the–NH_2 groups on the backbone of CS. Moreover, TPP solution donated some extent of the hydroxide ions, besides phosphoric ions [33]. Therefore, when the liberated H^+ions from the acetic acid were not sufficient to neutralize the hydroxide ions ($–OH^-$) of TPP, the$–OH^-$ ions would then tend to ionically cross-link with the protonated–NH_3^+groups of CS [35] and thus, resulted in reduction of the zeta potential of CS-TPP-NPs [34].

In addition, fig. 1c indicated a linear increase in PDI of CS-TPP-NPs from 0.29±0.02 to 0.76±0.05 by increasing the CS concentration from 0.5 to 5 mg/ml. The significant increase in the PDI of NPs is expected to be due to the fact that higher CS concentration tends to increase the agglomeration extent of CS-TPP-NPs which in turn predispose an increased poly dispersity of the particles. The CS-TPP-NPs obtained at CS concentration of 2 mg/ml were found to be optimal for further studies because of their smaller particle size (227±16 nm), higher zeta potential (+38±3 mV) and satisfactory PDI (0.31±0.05). TEM monograph, particle size distribution histogram and zeta potential histogram of CS-TPP-NPs prepared at 2 mg/ml and constant CS: TPP mass ratio (5:1), are presented in fig. 1d, 1e and 1f, respectively. TEM micrograph (fig. 1d) presents the round and smooth morphology of NPs with approximate mean particle size of 240 nm. The particle size histogram (fig. 1e) showed relatively narrow size distribution and approximate mean particle size of 227±16 nm. Similarly, zeta potential histogram (fig. 1f) presents narrow zeta potential distribution with approximate zeta potential of+38±3 mV.

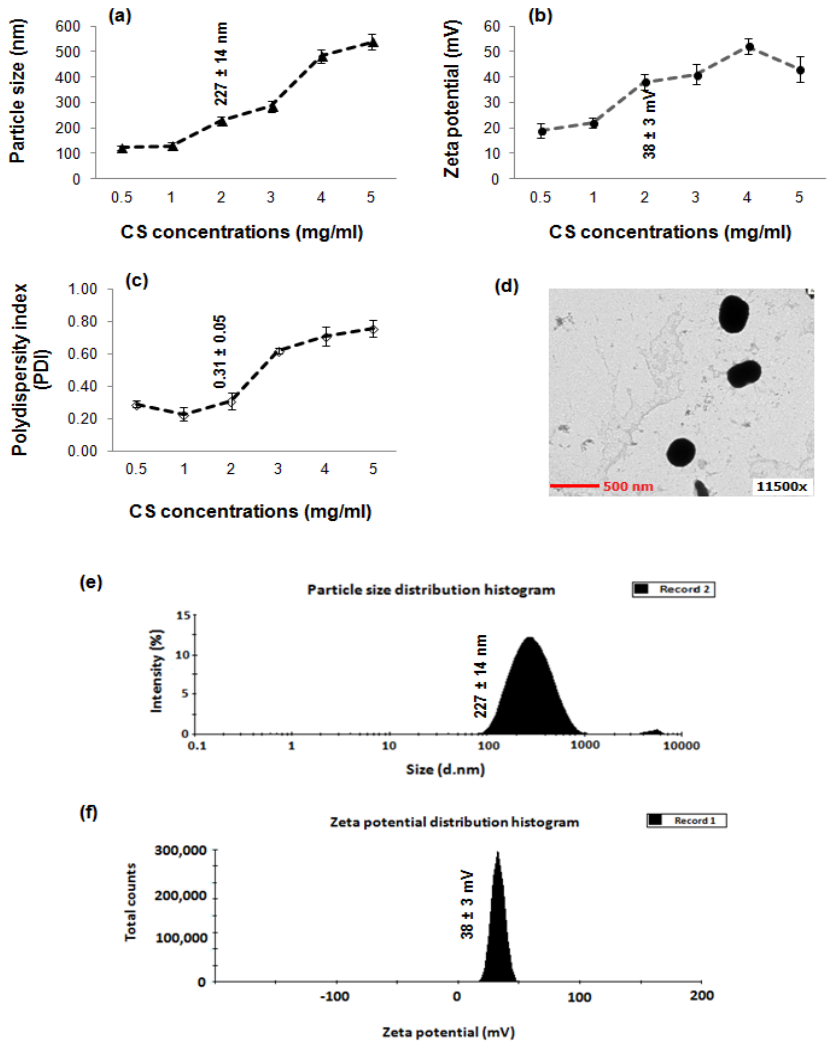

Fig. 1: Effect of CS concentration on (a) particle size (b) zeta potential (c) PDI of CS-TPP-NPs (d) TEM micrograph of CS-TPP-NPs with optimal characteristics at CS concentration of 2 mg/ml (e) size distribution by intensity showing 227±14 nm particle size, and (f) zeta potential distribution histogram showing 38±3 mV zeta potential (CS: TPP mass ratio 5:1, initial pH of CS solution 4.8, de acetylation degree of CS 85%)

Optimization of CS: TPP mass ratio

CS: TPP mass ratio is also one of the prime parameter to control the particle size, size distribution and zeta potential. A wide range, 2:1 to 10:1 of CS: TPP mass ratios were evaluated with constant CS concentration (2 mg/ml) as shown in fig. 2. The particle size was greatest for the lowest CS: TPP mass ratio (2:1) and decreased linearly by increasing CS: TPP mass ratio to 8:1 (fig. 2a). The results were also in agreement with previously published data [26]. Hu and co-workers reported that at higher TPP concentration the suspension became more turbid indicating the formation of particle agglomerates when superfluous TPP connect individual nano particles. At mass ratio 2:1 the aggregation is so intense that the particles precipitated immediately resulting in bigger particle size of 695±29 nm. The superfluous TPP linked the residual positively charged groups of separate CS-TPP-NPs resulting in aggregation. The particle size becomes larger again from 213±32 to 284±31 nm by increasing CS: TPP mass ratio from 9:1 to 10:1. This increment in the particle size might be caused by the possible electrostatic interaction (promoting aggregate formation) between the NPs because of a decrease in zeta potential of NPs that occurred as the CS: TPP mass ratios increased. The wide range of TPP concentrations that form particles is due to the fact that TPP can create as many as five ionic cross-links with amino groups of CS resulting in formation of individual particle or aggregate [21].

Fig. 2b on the other hand indicates that the zeta potential of CS-TPP-NPs was linearly increased from+12±3 to+34±1.5 mV, when the CS: TPP mass ratios were increased from 2:1 to 6:1. The increasing trend in zeta potential is expected to be caused by the variable cross-linking extent between the individual opposite charges donated by CS ($-NH_3^+$) and TPP ($-P_3O_{10}^{-5}$) at various CS: TPP mass ratios. Similarly, the number of individual charges ($-NH_3^+$and$-P_3O_{10}^{-5}$) and the corresponding charge density of both CS and TPP ions also imparted a great impact on the ionic interaction and thus on the zeta potential of NPs. For example, at a lower CS: TPP mass ratio (2:1), the TPP solution might donate a larger number of negative ions ($-P_3O_{10}^{-5}$), which could sufficiently neutralize the positive charges ($-NH_3^+$) on the contour of CS, and thus result in a lower zeta potential and vice versa, as shown in fig. 2b. The zeta potential was then decreased from+34±1.5 to+26±2 mV by increasing CS: TPP mass ratio from 6:1 to 10:1, respectively.

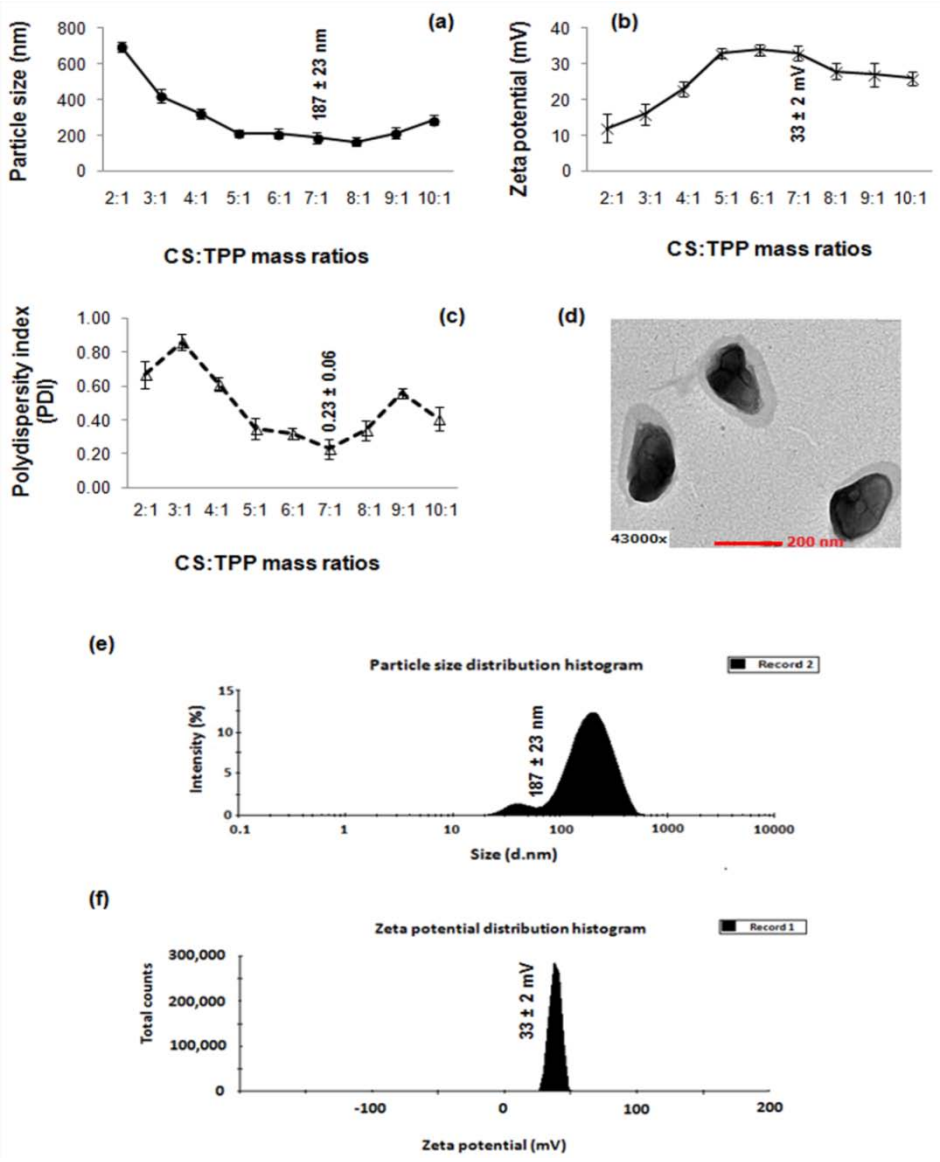

Fig. 2: Effect of CS: TPP mass ratios on (a) particle size (b) zeta potential (c) PDI of CS-TPP-NPs (d) TEM micrograph of CS-TPP-NPs with optimal characteristics at CS: TPP mass ratio of 7:1 (e) size distribution by intensity showing 187±23 nm particle size, and (f) zeta potential distribution histogram showing 33±2 mV zeta potential (CS concentration of 2 mg/ml, pH of CS solution 4.8, de acetylation degree of CS 85%)

Fig. 2c presented size distribution (PDI) of CS-TPP-NPs from 0.23±0.06 to 0.86±0.05 at various CS: TPP mass ratios (2:1 to 10:1). The anecdotal size distribution is expected to be due to variable cross-linking extent of TPP and CS ions that might resulted in variability in particle agglomeration. Further analysis revealed that CS-TPP-NPs obtained at 7:1 were best possible for further studies because of their relatively smaller particle size (187±32 nm) with narrow size distribution range (0.23±0.06) and higher zeta potential (+33±2 mV). These particles were further elaborated by TEM analysis (fig. 2d), particle size distribution histogram (fig. 2e) and zeta potential distribution histogram (fig. 2f). TEM micrograph (fig. 2d) showed smooth and regular conformation of NPs with approximate mean particle size of 200 nm. The particle size histogram (fig. 2e) showed relatively narrow size distribution and approximate mean particle size of 187±32 nm. Similarly, zeta potential histogram (fig. 2f) presents narrow zeta potential distribution with approximate zeta potential of+33±2 mV.

Optimizations of initial pH of CS solution

The initial pH of CS solution is an important environmental variable affecting the physicochemical characteristics of the prepared CS-TPP-NPs. The solubilisation of CS, a weak poly base, is reliant to the protonation extent of the NH_2 group when dissolved in acidic media. Since the extent of NPs formation is associated with the ionic cross-linking between CS and TPP, it is rational to conclude the effect of initial pH of CS solution on the characteristics of NPs [36].

Fig. 3 showed the variation of particle size, size distribution and zeta potential of CS-TPP-NPs at a range of initial pH values of the CS solution. The data obtained showed that the average particle size of CS-TPP-NPs was linearly increased from 112±19 to 167±17 nm, when the initial pH of CS solution was increased from 3.0 to 5.0 (fig. 3a). The increase in the particle size was sharp ($p<0.05$, paired t-test), when the initial pH of CS solution was increased from 5.5 (198±27 nm) to 7.0 (498±37 nm). Authors expect that the ionization of CS was optimal for cross-linking with TPP ions when the initial pH of CS solution was lower than 5.5 (3.0 to 5.0), and the protonation extent of the amino groups reduced as the pH of CS solution was increased above 5.5 (near to CS pKa 6.5), resulting in agglomeration and therefore formation of bigger particle sizes. The protonation of CS is the key characteristic of CS to give higher surface charge to NPs that resulted in higher extent of electrostatic repulsion. Therefore, particle aggregation may result from reduced repulsive potential on the surface of dispersed NPs when the initial pH of CS solution was increased.

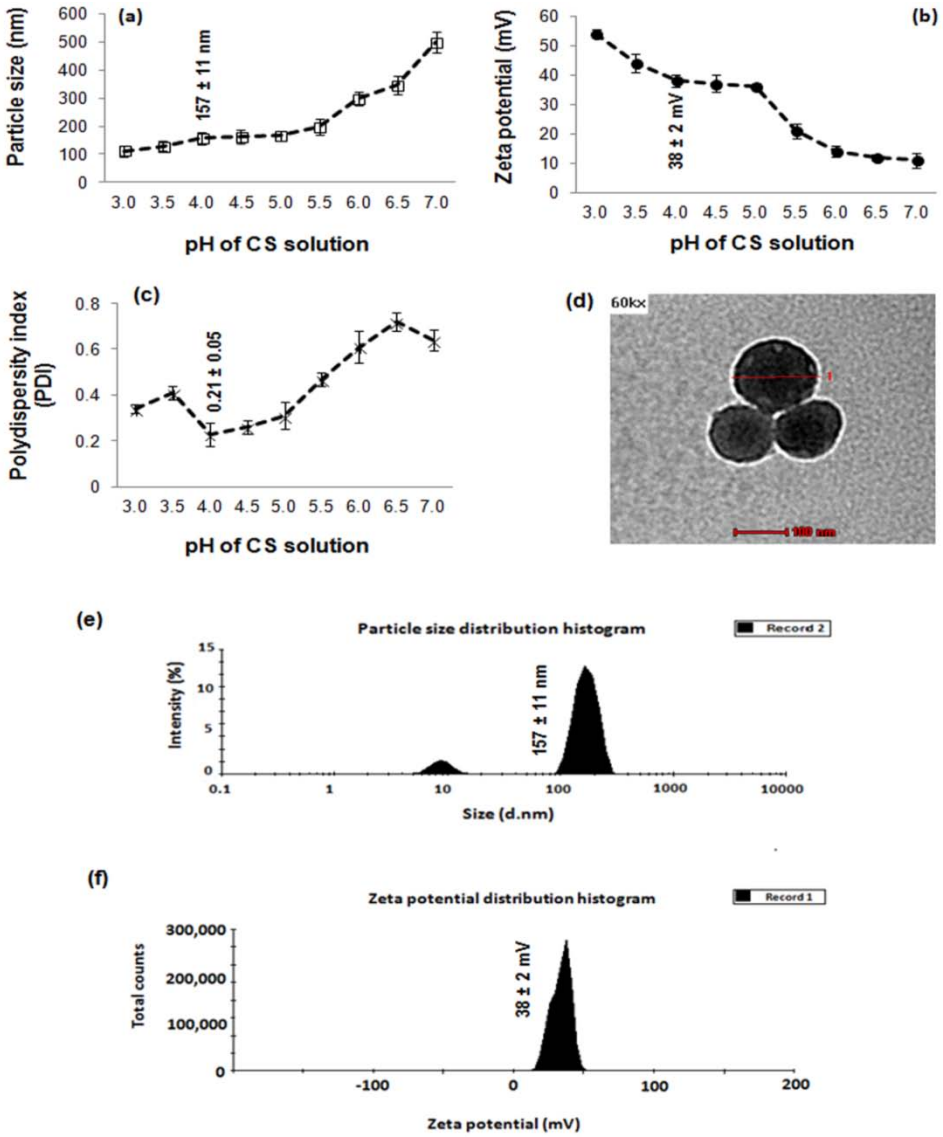

Fig. 3: Effect of initial pH of CS solution on (a) particle size (b) zeta potential (c) PDI of CS-TPP-NPs (d) TEM micrograph of CS-TPP-NPs with optimal characteristics at initial pH of CS solution of 4.0 (e) size distribution by intensity showing 157±11 nm particle size, and (f) zeta potential distribution histogram showing 38±2 mV zeta potential (CS concentration of 2 mg/ml, CS: TPP mass ratio of 7:1, de acetylation degree of CS 85%)

Data obtained also indicated a significant ($p<0.05$, paired t-test) reduction in the zeta potential from+54±3 to+11±2.5 mV, when the initial pH of CS solution was increased from 3.0 to 7.0 (fig. 3b). The decline in zeta potential of CS-TPP-NPs is expected to be due to a decrease in the proto-nation extent of–NH_2 groups on the backbone of CS by increasing the initial pH of CS solution from acidic (3.0) to neutral (7.0). The formation of NPs is strongly associated with ionic cross-linking and proto-nation extent of CS and TPP. These findings were also in accordance with the previously reported data [37]. Sung and co-workers reported that the degree of proto-nation (proto-nation extent) on the backbone of CS was observed to be decreased by increasing the initial pH of CS solution. At higher pH values (6.0 to 7.0), most of the amino groups on the backbone of CS were in–NH_2 form and did not contribute to the surface charge of the CS-TPP-NPs. Conversely, at low pH values (less than 5), most of the–NH_2 groups on CS were proto-nated (–NH_3^+) and imparted a net positive influence to the surface charge of the NPs. The particle size distribution data also highlighted a considerable increase in the side distribution range of CS-TPP-NPs from 0.23±0.05 to 0.72±0.04 at various pH values of CS solution (fig. 3c). The significantly wider range of size distribution range might be correlated with variable extent of proto-nation of CS and TPP at a range of initial pH of CS solution. After a sufficient data analysis, authors believed that at the initial pH of 4.0 of CS solution, the CS-TPP-NPs obtained were relatively smaller particle size (157±21 nm) with narrow size distribution (0.31±0.06) and higher surface charge (+38±2 mV). These particles were further elaborated by showing TEM analysis (fig. 3d), particle size distribution histogram (fig. 3e) and zeta potential distribution histogram (fig. 3f). TEM micrograph (fig. 3d) showed the NPs with round and smooth morphology with approximate mean particle size of ~150 nm. The particle size distribution histogram (fig. 3e) showed relatively narrow size distribution and approximate mean particle size of 157±21 nm. Similarly, zeta potential histogram (fig. 3f) presents narrow zeta potential distribution with approximate zeta potential of+38±2 mV.

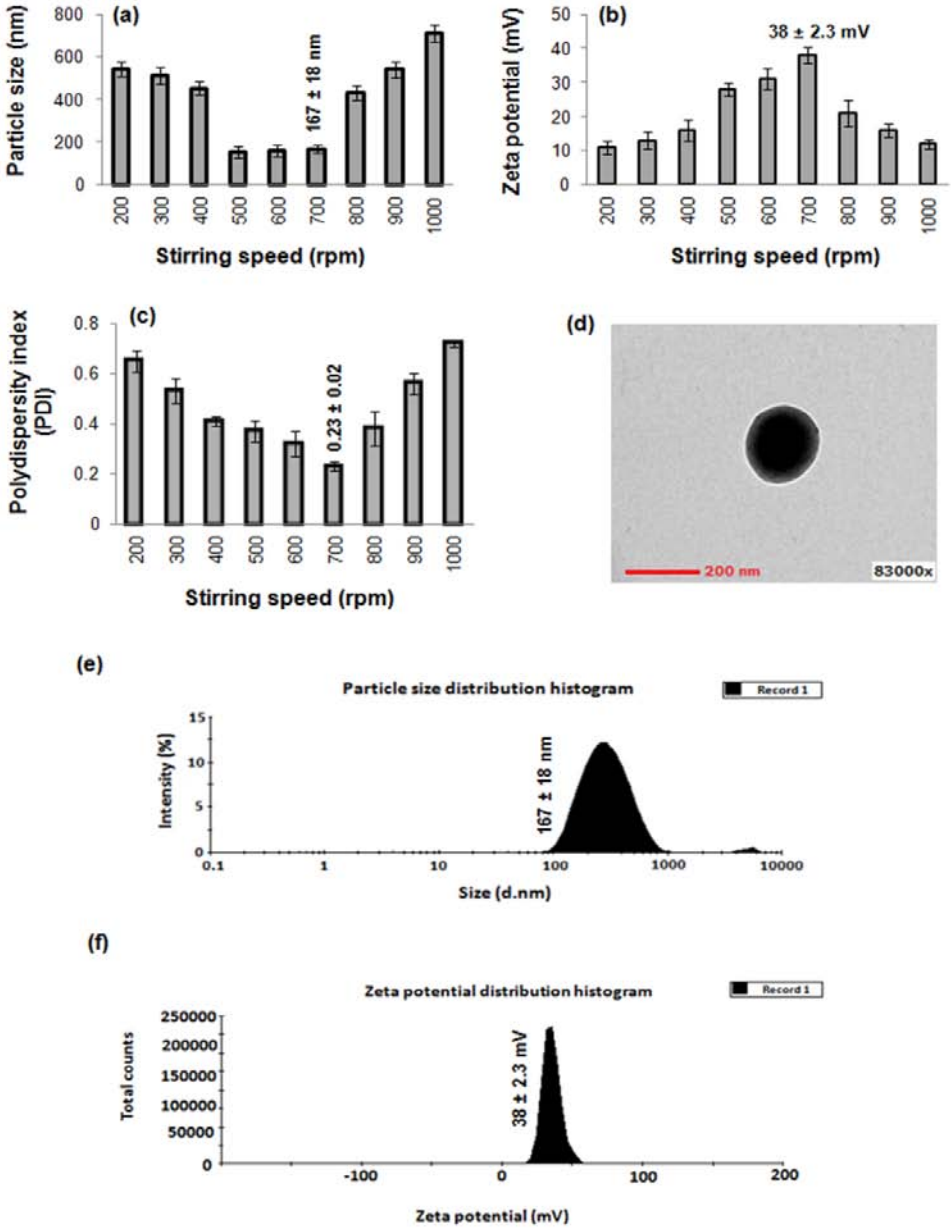

Fig. 4: Effect of stirring speed on (a) particle size (b) zeta potential (c) PDI of CS-TPP-NPs (d) TEM micrograph of CS-TPP-NPs with optimal characteristics at stirring speed of 700 rpm (e) size distribution by intensity showing 167±18 nm particle size, and (f) zeta potential distribution histogram showing 38±2.3 mV zeta potential (CS concentration of 2 mg/ml, CS: TPP mass ratio of 7:1, initial pH of CS solution of 4.0, de acetylation degree of CS 85%)

Optimizations of stirring speed

The results clearly showed that stirring rate impart a significant impact on the particle size, zeta potential and poly dispersity index of the resulting NPs as shown in fig. 4. The mean particle size reduced gradually from 543±32 nm to 453±31 nm, when the stirring speed increased from 200 rpm to 400 rpm (fig. 4a). However, further increase in stirring speed from 400 rpm to 700 rpm, result in a significant ($p<0.05$, paired t-test) decrease in the average particle size from 453±31 nm to 167±18 nm. Further increase in stirring speed from 800 rpm to 1000 rpm however, resulted in a significant increment in the particle size from 432±34 nm to 712±42 nm, respectively. The results were also in agreement with previously published study [33, 38], which reported significant impact of stirring speed on the particle size and size distribution of nano-carriers. Fan and co-workers [33] also reported that the particle size distribution was significantly narrowed by increasing the stirring speed from 200 rpm to 800 rpm, although aggregates were observed at 1000 rpm. The authors suggested that adequate stirring can accelerate the dispersion of TPP in chitosan solution and the increased shear force helps to narrow dispersity index; however, intense stirring may destroy the repulsive force between particles and lead to the aggregation of the particles. Together, the stir has impact on all the steps related to the crystallization process, including mixing, nucleating, growth and particle agglomeration. Compared to the low and high stirring speeds, the moderate stirring rate observed to improve the mixing and creates more uniform environment for NPs formation, therefore the resulting in particles that exhibit narrow dispersity. These results can also be observed through PDI analysis which highlights a gradual decrease in the dispersity range of CS-TPP-NPs from 0.65±0.04 to 0.23±0.02, when the stirring speed was increased from 200 rpm to 700 rpm (fig. 4c). However, an increase in the PDI above 700 rpm stirring speed might be exhibited by the particle agglomeration [39].

Moreover, resulting data also highlighted the effect of stirring speed on the zeta potential of CS-TPP-NPs as shown in fig. 4b. The zeta potential was observed to be increased gradually from+11±2 mV to+38±2.3 mV, when the stirring speed was increased from 200 rpm to 700 rpm. However, further increase in the stirring speed from 700 rpm to 800 rpm was resulted in a significant ($p<0.05$, paired t-test) decline in the zeta potential from+38±2.3 mV to+21±4 mV. The zeta potential was further reduced to+12±1.5 mV by increasing the stirring speed to 1000 rpm (fig. 4b). The decrease in the zeta potential above 700 rpm is expected to be due to the agglomeration of individual particles that tends to reduce surface area and the zeta potential associated with that surface. In this study, the stirring speed of 700 rpm was observed to be optimum condition to produce finest CS-TPP-NPs with relatively smaller particle size (167±18 nm), higher zeta potential (+38±2.3 mV) and narrow size range (0.23±0.02). Thus, the CS-TPP-NPs produced at 700 rpm were further assessed by TEM micrograph (fig. 4d), particle size histogram (fig. 4e) and zeta potential histogram (fig. 4f). TEM micrographs revealed that the self-aggregated CS-TPP-NPs will generally exhibit smooth and spherical morphology with approximate mean particle size of ~180 nm. According to the size distribution scale, the approximate mean particle size of these NPs was 167±18 nm nm as shown in fig. 4d. The zeta potential distribution histogram (fig. 4f) showed relatively narrow zeta potential distribution with approximate zeta potential of+38±2.3 mV.

Optimization of stirring period

This experiment was performed to investigate the effect of stirring time on colloidal characteristics of CS-TPP-NPs. Fig. 5 depicts the correlation between stirring time and various physicochemical characteristics of NPs such particle size, zeta potential and PDI. The resulting data clearly indicate the influence of stirring time by showing a gradual increase in the mean particle size from 156±21 nm to 176±61 nm, when the stirring time was increased from 0 to 10 min (fig. 5a). The increase in the particle size was sharp ($p<0.05$, paired t-test), when the stirring time was increased from 10 to 15 min. Fig. 5a highlights that the increase in the mean particle of NPs was more prominent when the stirring time was increased from 25 min to 30 min. However, this increasing trend in the average diameter of CS-TPP-NPs reached to 761±34 nm, when the NPs dispersion was stirred for 60 min. These findings were also supported by a previously published research [40], which reported an increasing trend in the mean particle size of NPs subjected to various stirring times with subsequent decreasing trend in the particle size. Nie and co-workers [40] demonstrated that the increase in the stirring time predisposes to the particle growth and the agglomeration processes, which resulted in an increased in the mean particle size gradually.

Similarly, fig. 5b showed a significant impact of the stirring time on the mean particle size, zeta potential and particle size distribution range of the resulting CS-TPP-NPs. The results revealed that the zeta potential of the resulting NPs was gradually decreased from+38±2 mV to+9±2 mV over the extended stirring period. The decrease in the zeta potential of CS-TPP-NPs by increasing stirring time is expected to be due to the agglomeration of individual particles that in turn reduce zeta potential. These results were also supported by the fig. 5c, which shows a fluctuating increasing trend in the dispersity index of the CS-TPP-NPs from 0.24±0.03 to 0.71±0.06, when the stirring time was increased from 0 to 60 min. This fluctuation in the PDI of NPs is expected to be due to the tendency of particles to form agglomerates or displace from the surface of each other. However, the analysis of resulting data revealed that the stirring time of 10 min was the optimum condition to prepare the CS-TPP-NPs with relatively smaller particle size (176±16 nm), higher zeta potential (+37±2.3 mV) and satisfactory range of size distribution (0.34±0.04). Therefore, these NPs were further characterized by microscopic examination (fig. 5d), particle size histogram (fig. 5e) and zeta potential histogram (fig. 5f). The microscopic micrographs revealed a rough and irregular morphology of the resulting NPs with approximate mean particle size of ~180 nm as shown in fig. 5d. The particle size distribution histogram showed relatively wider size distribution as indicated by smaller peak which showed 20% of the particle lower than 100 nm as shown in fig. 5e. The zeta potential distribution histogram (fig. 5f) showed narrow zeta potential distribution of NPs obtained at the stirring of 10 min with approximate zeta potential of+37±2.3 mV.

Effect of ultra-sonication

To assess the influence of ultra-sonication on the physicochemical characteristics of NPs, the prepared CS-TPP-NPs dispersion was subjected to high efficiency ultra-sonic processor over a serial time span from 0 to 12 min. Fig. 6 showed the effect of ultra-sonication duration on the mean particle size, zeta potential and size distribution range. The resulting data indicated a linear decreased in the average particle diameter of CS-TPP-NPs with an increased in sonication time (fig. 6a). A significant ($p<0.05$, paired t-test) reduction in the mean particle size was observed from 178±19 to 101±16 nm by the sonication of NPs dispersion from 0 to 4 min. The rate of decrement in the average particle size was reduced over the period of 4 to 15 min. Data analysis showed that the mean diameter of dispersed NPs was reduced by approximately 40% in initial 4 min of ultra-sonication with subsequent slow and linear reduction by 60% up to 15 min ultra-sonication. These results were also in accordance with Tang *et al.* [41] who reported that larger NPs were more susceptible to ultra-sonication compared to smaller NPs. The initial phase of size reduction, up to 4 min, can be attributed to the disruption of particles agglomerates formed during the synthesis of NPs. Nevertheless, the lower rate of size reduction in succeeding phase (4 to 15 min) of ultra-sonication was probably due to the degradation of the polymeric backbone of CS which also resulted in relaxation of the treated NPs. The authors believed that an extensive size reduction occurred in second phase of ultra-sonication might be due to the detachment of polymer parts from the NPs which might result in size reduction. This fact could also be explained by observing a decrease in PDI from 0.31±0.03 to 0.23±0.02 over the initial 4 min, with subsequent increase as the sonication time increases (fig. 6c).

Data obtained also signify a sharp reduction in the zeta potential of NPs from+41±2 to+22±2.4 mV in the initial 4 min of ultra-sonication. However, in the succeeding phase from 4 to 15 min, there was observed linear decrease in the zeta potential of CS-TPP-NPs as shown in fig. 6b. The decrease in the zeta potential could be attributed to the fragmentation of NPs structure. The findings were

also supported by previously published data [30] which had also highlighted a significant degradation of polymer during an ultra-sonication process. Floris and co-worker [30] further explained that the degradation of the polymer is mainly caused by cavitation effect. The resulting data revealed that moderate use of ultra-sonication could be able to reduce the particle size significantly *via* the disruption of particle aggregations. However, extensive ultra-sonication may cause severe fragmentation of the compact structure of the NPs subjected. The results were harmonised by observing TEM micrographs of CS-TPP-NPs at 0 and 15 min ultra-sonication as shown in fig. 6d and 6e, respectively. The obtained micrographs clearly showed that the NPs before ultra-sonication (fig. 6d) were spherical and smooth with compact surface morphology. Fig. 6e clearly indicated the deformation of spherically compact and smooth surface structure to rough, irregular and fragmented structure when the NPs, were subjected to ultra-sonication for 15 min.

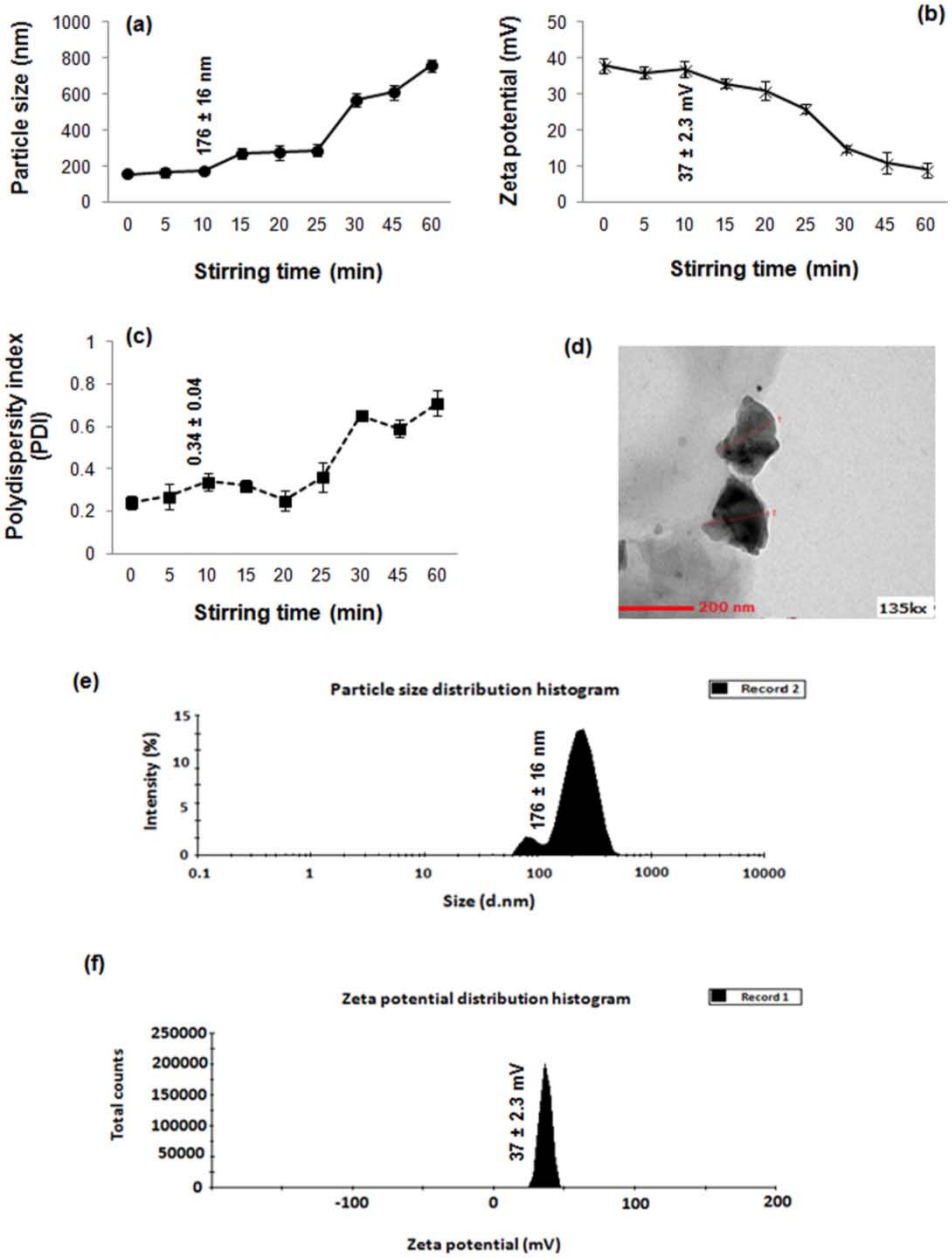

Fig. 5: Effect of stirring time on (a) particle size (b) zeta potential (c) PDI of CS-TPP-NPs (d) TEM micrograph of CS-TPP-NPs with optimal characteristics at stirring time of 10 min (e) size distribution by intensity showing 176±16 nm particle size, and (f) zeta potential distribution histogram showing 37±2.3 mV zeta potential (CS concentration of 2 mg/ml, CS: TPP mass ratio of 7:1, initial pH of CS solution of 4.0, stirring speed of 700 rpm, de acetylation degree of CS 85%)

Optimizations of ultra-centrifugation condition

Centrifugation is one of the integral process parameter affecting the particle size, zeta potential, PDI and percent actual yield of the NPs. In order to investigate its effect, centrifugation with different speeds (15 000 to 35 000 rpm) was applied to separate and sediment the disperse CS-TPP-NPs and agglomerates at a constant time period (30 min). Fig. 7 presents the particle size, zeta potential and size distribution of CS-TPP-NPs in supernatant and sediment obtained at various centrifugation speeds. At the lowest centrifugation speed (15 000 rpm), the NPs isolated in the supernatant and sediment had shown approximately similar mean particle size around 182±14 and 187±21 nm, respectively (fig. 7a). The mean particle size of NPs obtained in the supernatant was

significantly ($p<0.05$, paired t-test) reduced from 182±14 to 58±9 nm, when the ultra-centrifugation speed was increased from 15 000 rpm to 35 000 rpm. All the NPs larger than ~58±9 nm were isolated from the NPs dispersions at 35 000 rpm. On the other hand, the average particle size of the NPs isolated in sediments was increased from 187±21 nm to 392±36 nm as expected, at the diverse range of centrifugation speed (fig. 7a). The particle size of NPs obtained in the sediment was sharply increased when the centrifugation was performed above 25 000 rpm. Authors believed that the higher centrifugation speed (35 000 rpm) efficiently isolated all the bigger particles in the sediment and results in very small particles (~58±9 nm) remained in the supernatant. However, on the other side, higher centrifugation speed also tends to create the formation of particle agglomerates which resulted in a sharp increase in particle size in the sediments (fig. 7a). This could also be the reason for a significant increase in the PDI from 0.26±0.03 to 0.52±0.09, when the centrifugation speed was increased from 15 000 rpm to 35 000 rpm.

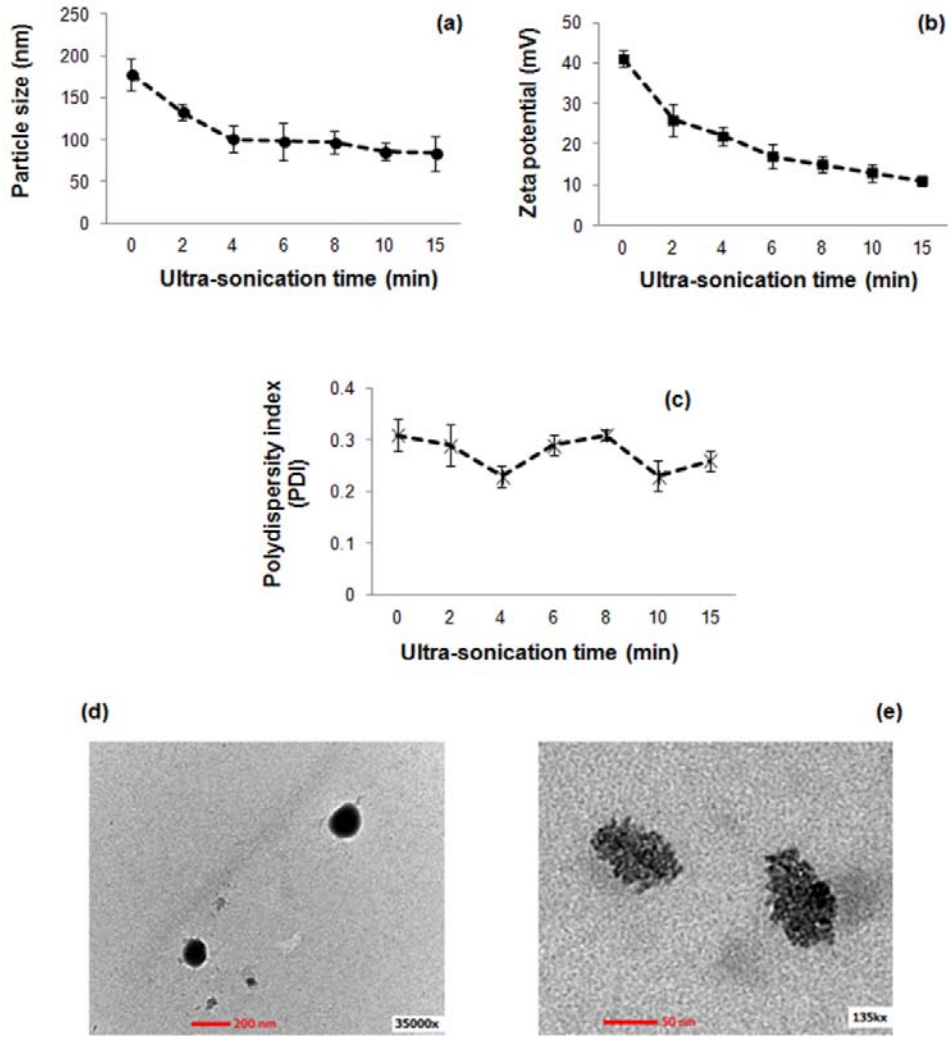

Fig. 6: Effect of ultra-sonication time on (a) particle size (b) zeta potential (c) PDI of CS-TPP-NPs (d) TEM micrograph of CS-TPP-NPs at ultra-sonication time of 0 min and (e) TEM micrograph of CS-TPP-NPs at ultra-sonication time of 15 min (CS concentration of 2 mg/ml, CS: TPP mass ratio of 7:1, initial pH of CS solution of 4.0, stirring speed of 700 rpm for 10 min, de acetylation degree of CS 85%)

Fig. 7b depicts that the zeta potential of the NPs in the supernatant was reduced from+31±2 to+28±3 mV, when the centrifugation speed was increased from 15 000 rpm to 20 000 rpm. However, a sharp reduction in the zeta potential was observed at the centrifugation speed of 25 000 rpm and above (fig. 7b). It is expected to be due to the fact that at higher centrifugation speed (25 000 to 35 000 rpm), only very small particles remained in the supernatant, having lower average zeta potential. Conversely, the zeta potential of NPs was linearly increased from+24±2 to+32±2.1 mV in the sediment, when the centrifugation speed was increased from 15 000 rpm to 25 000 rpm. It means that almost all the bigger particles have been isolated in the sediment at higher centrifugation speed which imparted greater value of the zeta potential. However, a considerable decrease in the zeta potential of the NPs isolated at 30 000 rpm and 35 000 rpm might be caused by the particle agglomeration which occurred at higher centrifugation speeds (fig. 7b).

In addition, fig. 7c indicated the effect of centrifugation speed on the percent actual yield of the NPs. The resulting data clearly highlighted a slight increase in the percent actual yield of NPs from 13±2.9% to 16±1.8%, when the centrifugation speed was increased from 15 000 rpm to 20 000 rpm. The percent actual yield was increased sharply from 16±1.8 to 36±1.4%, when the centrifugation speed was increased from 20 000 rpm to 25 000 rpm. Afterward, a linear increase in the percent actual yield was observed when the centrifugation speed was increased from 30 000 rpm to 35 000 rpm. Though, the percent actual yield of the CS-TPP-NPs was highest at the centrifugation speed of 35 000; however, the tendency of particle agglomeration and lower zeta potential obtained at this centrifugation speed discouraged to claim it as the optimum condition. Hence, in our system, a centrifugation speed of 25 000 rpm was found to be optimum to isolate and centrifuge the dispersed NPs. At this centrifugation speed, the sediment of NPs had

shown minimal particle agglomeration as well as higher zeta potential and optimal percent actual yield of CS-TPP-NPs.

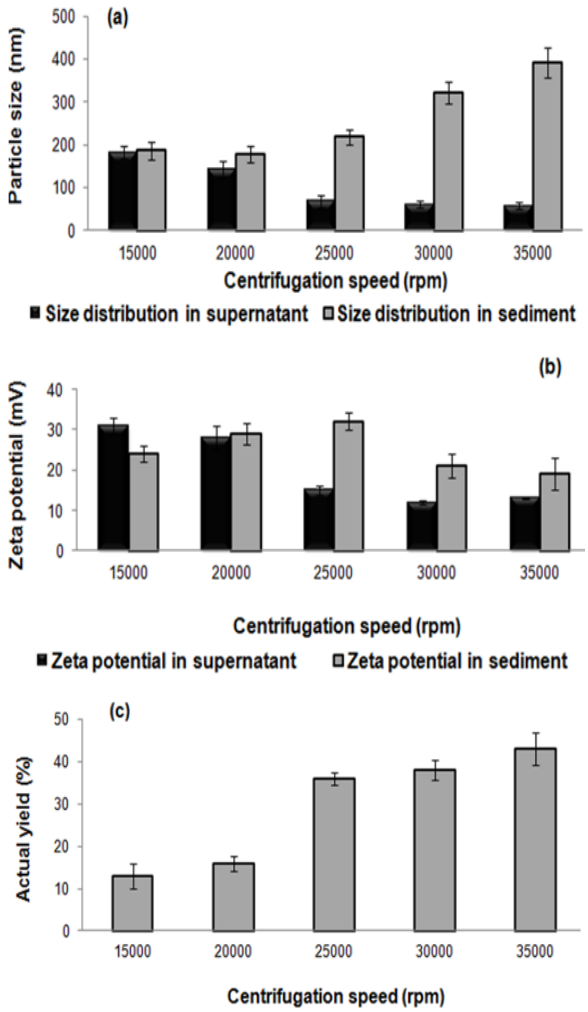

Fig. 7 Effect of ultra-centrifugation on (a) particle size in the supernatant (■) and NPs sediment (□), (b) zeta potential in the supernatant (■) and NPs sediment (□), (c) actual yield (%) of CS-TPP-NPs at various ultra-centrifugation speeds (CS concentration of 2 mg/ml, CS: TPP mass ratio of 7:1, initial pH of CS solution of 4.0, stirring speed of 700 rpm for 10 min, ultra-sonication for 4 min, de acetylation degree of CS 85%)

Optimal formulation and process parameters

After the optimization of different formulation and process parameters, the following conditions were retained: CS concentration of 0.2% w/v in 1% v/v acetic acid, CS: TPP mass ratio of 7:1, initial pH of CS solution of 4.0, stirring speed 700 rpm, stirring time 10 min and ultra-centrifugation at 25 000 rpm for 30 min. At these conditions, the mean particle size, zeta potential and PDI of CS-TPP-NPs were around 187±21 nm,+37±3.5 mV and 0.28±0.03, respectively.

Swelling characteristics

A series of experiments were executed to examine the effects of pH of the incubation media (PBS) on the physical characteristics of lyophilized CS-TPP-NPs prepared at optimal conditions. Fig. 8 presents the effect various pH of the incubating media (PBS) on the swelling characteristics of CS-TPP-NPs. The data obtained showed that the swelling ratio (25±2%) of NPs incubated at pH 3.0 was significantly ($p<0.05$, paired t-test) higher compared to the swelling ratios (13±1.5%) of the NPs incubated at pH 5.0. The trend was expected to be due to the fact that at low pH (e. g., pH 3.0), most of the amino groups on the backbone of CS were in the form of–NH_3^+, and thus, the overall charge on the surface of the NPs was positive. Therefore, authors believed that the extended swelling conformation of CS-TPP-NPs at low pH could be caused by a strong electrostatic repulsion among like charges (–NH_3^+groups) of CS. Additionally, the swelling conformation at low pH could also be the reason of bonding of–NH_3^+groups on the surface of CS with the surrounding water (water of hydration). In contrast, the lower extent of swelling at high pH values (4–5) could be caused by the fact that at this pH range, the amino groups in CS were less extensively protonated and the–PO_4^- groups of TPP were in ionized form. However, this still can produce some electrostatic attractions between CS and TPP in the NPs matrices to form compact structure and thus restrains the swelling of NPs. On the other hand, fig. 8 also showed the swelling conformation of NPs was greatly ($p<0.05$, paired t-test) increased from 27±2% to 39±3.5% at pH 6–8, respectively. This can be explained on the basis that at high pH values (6–8), most of the amino groups of CS were in the neutral form (–NH_2) due to the pKa value of CS (6.5) [42], while the PO_4^-groups of TPP were in the ionized form (–PO_4^-). Thus, the electrostatic attraction between CS and its counter ion (TPP) become weakened, which may result in increase in the swelling extent of CS-TPP-NPs as shown in fig. 8.

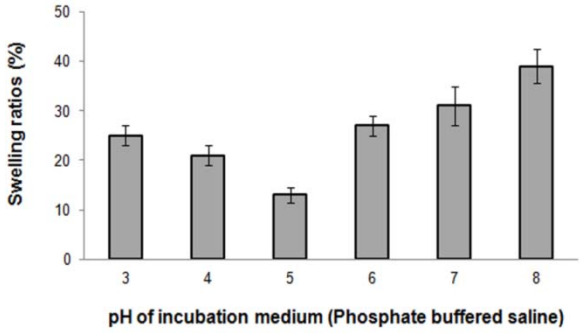

Fig. 8: Swelling ratios of CS-TPP-NPs at various pH values (3.0, 4.0, 5.0, 6.0, 7.0, and 8.0) of incubating medium (phosphate buffered saline, PBS), (CS concentration of 2 mg/ml, CS: TPP mass ratio of 7:1, initial pH of CS solution of 4.0, stirring speed of 700 rpm for 10 min, ultra-sonication for 4 min, deacetylation degree of CS 85%)

Colloidal stability on storage

The present experiment was conducted to assess the impact of storage on the physicochemical characteristics of CS-TPP-NPs prepared at optimal conditions. Fig. 9 showed the changing patterns of the mean particle size, zeta potential and size distribution over an extended storage period (day-0 to-day-32). The resulting data indicate a slight ($p>0.05$, paired t-test) increase in the mean particle size of CS-TPP-NPs from 174±21 nm (day-0) to 181±12 nm (day-4) as shown in fig. 9a. The mean particle size was increased noticeably from day-4 (181±12 nm) to-day-8 (214±27 nm); however from day-8 to-day-20, only a slight increase in the average diameter of NPs was observed (fig. 9a). A significantly ($p<0.05$, paired t-test) greater enlargement was observed in the mean particle size of CS-TPP-NPs from day-20 (232±31 nm) to-day-32 (487±12 nm). The sharp increase in the particle size of NPs could be attributed to the formation of particle agglomerates upon storage in PBS (pH, 7.4) at room temperature.

On the other hand, there was no change observed in the zeta potential of NPs between day-0 and upon storage up to day-4 as shown in fig. 9b. A considerable ($p<0.05$, paired t-test) decline in the zeta potential from+33±3.1 to+26±1.6 mV was observed from day-4 to-day-20. A further decrease in the zeta potential of CS-TPP-NPs was observed over the extend storage period from day-20 to-day-32 and this was thought to be caused by their interactions to form particle agglomerates in the storage media. The possible mechanism behind this trend could be the change in the amino groups (–NH_3^+)

on the surface of CS-TPP-NPs that may turn to neutral form (–NH_2) upon storage in media with alkaline pH (7.4). This may in turn reduce the electrostatic attraction between the amino groups (–NH_3^+) on the contour of CS and its TPP counter ion (–PO_4^-) and thus result in loosening of compact structure and particle enlargement. This could also be attributed to the fact that decrease in the positive charge caused by the conversion of–$NH_3^+$to–NH_2 groups on the surface of NPs may in turn reduced the electrostatic repulsion between dispersed NPs and thus tend to the formation of particle agglomerates. This phenomenon can be also supported from size distribution results (fig. 9c), showing consistent increase in the PDI of particles above than day-4. The significant increased in the PDI of CS-TPP-NPs from 0.23±0.02 (day-4) to 0.76±0.06 (day-32) is expected to be due to the particle aggregation. The results were further elaborated by TEM analysis of CS-TPP-NPs at day-0 (fig. 9d) and day-32 (fig. 9e), highlighting increase in particle size upon agglomeration. TEM micrographs showed that the prepared NPs were round and smooth in morphology with approximate mean particle size of 180 nm, before storage in PBS (pH, 7.4) (fig. 9d). However, after storage for 32 d, the TEM micrograph showed noticeable particle aggregation and significant increase in the approximate particle size to 500 nm as shown in fig. 9e.

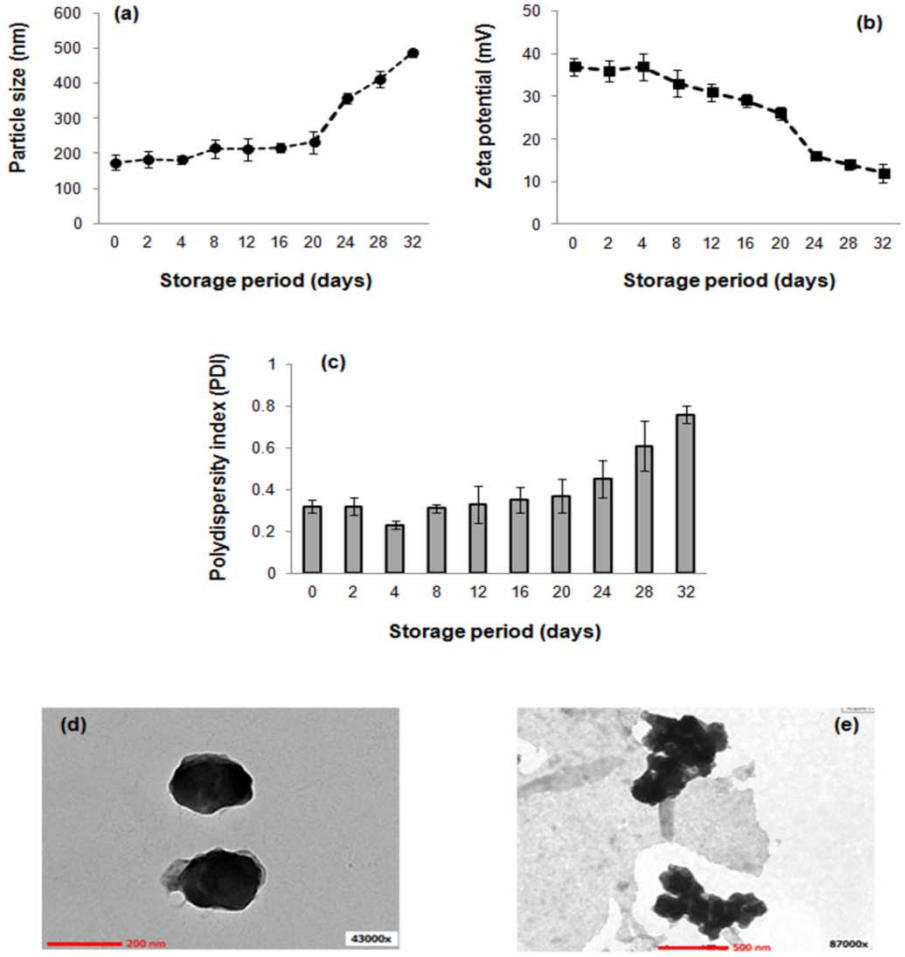

Fig. 9: Colloidal stability of CS-TPP-NPs on storage in terms of (a) particle size (b) zeta potential (c) PDI (CS concentration of 2 mg/ml, CS: TPP mass ratio of 7:1, initial pH of CS solution of 4.0, stirring speed of 700 rpm for 10 min, ultra-sonication for 4 min, de acetylation degree of CS 85%)

CONCLUSION

The present study was aimed to investigate the impact of formulation and process parameters on the physicochemical characteristics of CS-TPP-NPs. The resulting data clearly verified a significant influence of the preparation conditions (CS concentration, CS: TPP mass ratio, pH of CS solution) and process parameters (stirring speed, stirring time, ultra-sonication and ultra-centrifugation) on the mean particle size, zeta potential and size distribution index of CS-TPP-NPs. The controlling parameters are clearly identified in the present study in order to produce the CS-TPP-NPs with optimal characteristics and provide an opportunity for manipulating and optimizing the nano particle for further intended pharmaceutical and nutraceuticals applications.

ACKNOWLEDGEMENT

The authors gratefully acknowledge the Ministry of Higher Education, Malaysia, and Universiti Kebangsaan Malaysia, for support and funding current project. The authors would also like to acknowledge Universiti Teknologi MARA (UiTM), Puncak Alam Campus, Malaysia, for support and providing resources to write this article.

CONFLICT OF INTERESTS

The authors report no declaration of interest in the current research work.

REFERENCES

1. Lademann J, Richter H, Teichmann A, Otberg N, Blume-Peytavi U, Luengo J, *et al.* Nanoparticles–an efficient carrier for drug delivery into the hair follicles. Eur J Pharm Biopharm 2007;66:159–64.
2. Alvarez-Roman R, Barre G, Guy RH, Fessi H. Biodegradable polymer nano capsules containing a sunscreen agent: preparation and photoprotection. Eur J Pharm Biopharm 2001; 52:191–5.
3. Colonna C, Conti B, Perugini P, Pavanetto F, Modena T, Dorati R, *et al.* Ex vivo evaluation of prolidase loaded chitosan

nanoparticles for the enzyme replacement therapy. Eur J Pharm Biopharm 2008;70:58–65.

4. Lee PW, Peng SF, Su CJ, Mi FL, Chen HL, Wei MC, *et al.* The use of biodegradable polymeric nanoparticles in combination with a low-pressure gene gun for transdermal DNA delivery. Biomaterials 2008;29:742–51.
5. Alvarez-Roman R, Naik A, Kalia YN, Guy RH, Fessi H. Enhancement of topical delivery from biodegradable nanoparticles. Pharm Res 2004;21:1818–25.
6. Kuchler S, Radowski MR, Blaschke T, Dathe M, Plendl J, Haag R, *et al.* Nanoparticles for skin penetration enhancement–a comparison of a dendritic core-multishell-nano-transporter and solid lipid nanoparticles. Eur J Pharm Biopharm 2009;71:243–50.
7. Wu X, Price GJ, Guy RH. Disposition of nanoparticles and an associated lipophilic permeant following topical application to the skin. Mol Pharmacol 2009;6:1441–8.
8. Katas H, Hussain Z, Ling TC. Chitosan nanoparticles as a percutaneous drug delivery system for hydrocortisone. J Nanomater 2012. Doi: 10.1155/2012/372725. [Article in Press]
9. Hussain Z, Katas H, Amin MCIM, Kumolosasi E, Buang F, Sahudin S, *et al.* Self-assembled polymeric nanoparticles for percutaneous co-delivery of hydrocortisone/hydroxytyrosol: an ex vivo and *in vivo* study using an NC/Nga mouse model. Int J Pharm 2013;444:109-19.
10. Agnihotri SA, Mallikarjuna NN, Aminabhavi TM. Recent advances on chitosan-based micro-and nanoparticles in drug delivery. J Controlled Release 2004;100:5–28.
11. Zhang H, Oh M, Allen C, Kumacheva E. Monodisperse chitosan nanoparticles for mucosal drug delivery. Biomacromolecules 2004;5:2461–8.
12. Rinaudo M. Chitin and chitosan: properties and applications. Prog Polym Sci 2006;31:603–32.
13. De Moura MR, Aouada FA, Avena-Bustillos RJ, McHugh TH, Krochta JM, Mattoso LH, *et al.* Improved barrier and mechanical properties of novel hydroxypropylmethyl-cellulose edible films with chitosan/tripolyphosphate nanoparticles. J Food Eng 2009;92:448–53.
14. Gan Q, Wang T, Cochrane C, McCarron P. Modulation of surface charge, particle size and morphological properties of chitosan–TPP nanoparticles intended for gene delivery. Colloids Surf B 2005;44:65–73.
15. Calvo P, Remu˜nán-López C, Vila-Jato JL, Alonso MJ. Novel hydrophilic chitosan–polyethylene oxide nanoparticles as protein carriers. J Appl Polym Sci 1997;63:125–32.
16. Huang Y, Lapitsky Y. Monovalent salt enhances colloidal stability during the formation of chitosan/tripolyphosphate microgels. Langmuir 2011;27:10392–9.
17. Yang HC, Hon MH. The effect of the degree of deacetylation of chitosan nanoparticles and its characterization and encapsulation efficiency on drug delivery. Polym Plast Technol Eng 2010;49:1292–6.
18. López-León T, Carvalho ELS, Seijo B, Ortega-Vinuesa JL, Bastos-González D. Physicochemical characterization of chitosan nanoparticles: electrokinetic and stability behavior. J Colloid Interface Sci 2005;283:344–51.
19. Sinha V, Singla A, Wadhawan S, Kaushik R, Kumria R, Bansal K, *et al.* Chitosan microspheres as a potential carrier for drugs. Int J Pharm 2004;274:1–33.
20. Wu Y, Yang W, Wang C, Hu J, Fu S. Chitosan nanoparticles as a novel delivery system for ammonium glycyrrhizinate. Int J Pharm 2005;295:235–45.
21. Papadimitriou S, Bikiaris D, Avgoustakis K, Karavas E, Georgarakis M. Chitosan nanoparticles loaded with dorzolamide and pramipexole. Carbohydr Polym 2008;73:44–54.
22. Hussain Z, Katas H, Amin MCIM, Kumulosasi E, Sahudin S. Antidermatitic perspective of hydrocortisone as chitosan nanocarriers: an ex vivo and *in vivo* assessment using an NC/Nga mouse model. J Pharm Sci 2013;102:1063–75.
23. Grenha A, Seijo B, Remu˜nán-López C. Microencapsulated chitosan nanoparticles for lung protein delivery. Eur J Pharm Sci 2005;25:427–37.
24. Gan Q, Wang T. Chitosan nanoparticle as protein delivery carrier—systematic examination of fabrication conditions for efficient loading and release. Colloids Surf B 2007;59:24–34.
25. Papadimitriou SA, Achilias DS, Bikiaris DN. Chitosan-g-PEG nanoparticles ionically cross-linked with poly(glutamic acid) and tri polyphosphate as protein delivery systems. Int J Pharm 2012;430:318–27.
26. Hu B, Pan C, Sun Y, Hou Z, Ye H, Hu B, et al. Optimization of fabrication parameters to produce chitosan–tripolyphosphate nanoparticles for delivery of tea catechins. J Agric Food Chem 2008;56:7451–8.
27. Luo Y, Zhang B, Cheng WH, Wang Q. Preparation, characterization and evaluation of selenite-loaded chitosan/TPP nanoparticles with or without zein coating. Carbohydr Polym 2010;82:942–51.
28. Keawchaoon L, Yoksan R. Preparation, characterization and *in vitro* release study of carvacrol-loaded chitosan nanoparticles. Colloids Surf B 2011;84:163–71.
29. Csaba N, Köping-Höggård M, Alonso MJ. Ionically crosslinked chitosan/tripolyphosphate nanoparticles for oligonucleotide and plasmid DNA delivery. Int J Pharm 2009;382:205–14.
30. Floris A, Meloni MC, Lai F, Marongiu F, Maccioni AM, Sinico C, *et al.* Cavitation effect on chitosan nanoparticle size: a possible approach to protect drugs from ultrasonic stress. Carbohydr Polym 2013;94:619–25.
31. Dai ZZ, Yin JB, Yan SF, Cao T, Ma J, Chen XS, *et al.* Polyelectrolyte complexes based on chitosan and poly (L-glutamic acid). Polym Int 2007;56:1122–7.
32. Liu H, Gao C. Preparation and properties of ionically cross-linked chitosan nanoparticles. Polym Adv Technol 2009;20:613–9.
33. Fan W, Yan W, Xu Z, Ni H. Formation mechanism of monodisperse, low molecular weight chitosan nanoparticles by ionic gelation technique. Colloids Surf B 2012;90:21–7.
34. Qun G, Ajun W. Effects of molecular weight, degree of acetylation and ionic strength on surface tension of chitosan in dilute solution. Carbohydr Polym 2006;64:29–36.
35. Shu XZ, Zhu KJ. The influence of multivalent phosphate structure on the properties of ionically cross-linked chitosan films for controlled drug release. Eur J Pharm Biopharm 2002;54:235–43.
36. Ko J, Park H, Hwang S, Park J, Lee J. Preparation and characterization of chitosan microparticles intended for controlled drug delivery. Int J Pharm 2002;249:165–74.
37. Sung TL, Fwu LM, Yu JS, Shin SS. Equilibrium and kinetic studies of copper (II) ion uptake by chitosan-tripolyphosphate chelating resin. Polymer 2001;42:1879–92.
38. Zhu HJ, Liu XM, Yangn H, Shen XD. Effect of the stirring rate on physical and electrochemical properties of LiMnPO4 nanoplates prepared in a polyol process. Ceram Interfaces 2014;40:6699–704.
39. Nazeri N, Avadi MR, Faramarzi MA, Safarianc S, Tavoosidana G, Khoshayande MR, *et al.* Effect of preparation parameters on ultra low molecular weight chitosan/hyaluronic acid nanoparticles. Int J Biol Macromol 2013;62:642–6.
40. Nie KB, Wang XJ, Wu K, Xu L, Zheng MY, Hu XS, et al. Processing, microstructure and mechanical properties of magnesium matrix nanocomposites fabricated by semisolid stirring assisted ultrasonic vibration. J Alloys Compd 2011;509:8664–9.
41. Tang E, Huang M, Lim L. Ultrasonication of chitosan and chitosan nanoparticles. Int J Pharm 2003;265:103–14.
42. Wu YT, Grant CL. Effect of chelation chemistry of sodium polyaspartate on the dissolution of calcite. Chem Biomol Eng 2002;18:6813–20.